



Dynamic Windows Based on Reversible Metal Electrodeposition with Enhanced Functionality

Shakirul M. Islam, Christine N. Fini, and Christopher J. Barile *,^z

Department of Chemistry, University of Nevada, Reno, Nevada 89557, USA

Electronically tintable windows increase the energy efficiency and comfort of buildings and automobiles. Recently, dynamic windows harnessing reversible metal electrodeposition have been explored as a viable alternative to electrochromic materials. In this manuscript, we first construct 25 cm² dynamic windows with two tin-doped indium oxide (ITO) working electrodes, a metal frame counter electrode, and an aqueous-based electrolyte containing metal ions. This arrangement allows metal electrodeposition to occur simultaneously on both window panes and increases switching speed such that devices switch to ~30% transmission in 10 s compared to analogous windows with one working electrode which take 30 s to reach the same transmission value. Windows with two working electrodes switch between clear (~82% transmission at 600 nm) and black (~8% transmission at 600 nm) states within 30 s, making them among the fastest metal-based dynamic windows reported on this scale. Second, we elicit selective metal electrodeposition on Pt nanoparticles that are attached to ITO substrates via a self-assembled monolayer (SAM). By patterning the SAM of Pt nanoparticles, metal electrodeposition can be spatially controlled on both the macroscale and microscale. Taken together, these results demonstrate the versatility of the reversible metal electrodeposition architecture for dynamic windows.

© The Author(s) 2019. Published by ECS. This is an open access article distributed under the terms of the Creative Commons Attribution 4.0 License (CC BY, <http://creativecommons.org/licenses/by/4.0/>), which permits unrestricted reuse of the work in any medium, provided the original work is properly cited. [DOI: 10.1149/2.0961908jes]



Manuscript submitted February 6, 2019; revised manuscript received March 28, 2019. Published May 9, 2019.

Increasing the energy efficiency of buildings and automobiles is a crucial component of fostering the transition of our energy economy away from fossil fuels and toward renewable energy sources.¹ Dynamic windows, which possess electronically tunable transmission, are one promising technology to increase the energy efficiency of spaces. Previous studies have demonstrated that the incorporation of robust dynamic windows into buildings leads to a 10% average reduction in energy consumption due to heating, cooling, and lighting savings.^{2,3} Additionally, dynamic windows are more aesthetically pleasing than traditional window blinds and their switching can be automated.

Recently, dynamic windows utilizing reversible metal electrodeposition have emerged as an intriguing alternative to those based on other technologies such as electrochromic materials,^{4,5} polymer dispersed liquid crystals,^{6,7} and thermochromic materials.^{8,9} These windows function via the reversible electrochemical transfer of metal between a metal window frame and a transparent conducting pane.¹⁰ Advantages of metal-based dynamic windows include high optical contrast, color neutral switching, the use of nontoxic aqueous electrolytes, and the potential for manufacturing using low-cost solution-processed techniques.¹¹

One challenge hindering the practical adoption of metal-based dynamic windows is the difficulty of uniformly electroplating metals over a large electrode area.^{12,13} A self-assembled monolayer (SAM) of Pt nanoparticles was previously used to control the nucleation of metal electrodeposition on tin-doped indium oxide (ITO) surfaces.¹⁰ This approach allowed for the construction of 25 cm² dynamic windows that possess uniform metal electrodeposition, giving rise to uniform device tinting. Currently, these windows harness the electrodeposition of Cu from an aqueous-based gel electrolyte along with a second metal such as Bi or Ag.¹⁴

In this work, we expand upon the traditional metal-based dynamic window architecture to create dynamic windows with enhanced switching speed and functionality. In particular, we construct windows that elicit metal electrodeposition on both window panes to increase switching speed. We also design windows that facilitate selective reversible metal electrodeposition such that the devices darken in a tailored pattern on the macro and microscales.

Experimental

All chemicals were obtained from commercial sources and used as received. Electrochemical studies utilized a VSP-300 Biologic potentiostat. The current measured by the potentiostat was recorded every 100 ms. Half-cell experiments with three electrodes consisted of a “no-leak” Ag/AgCl (3 M KCl) reference electrode (eDAQ, Inc.), a Pt wire counter electrode, and a Pt-modified or unmodified ITO on glass working electrode (Xinyan Technology, 15 Ω sq⁻¹). Half-cell experiments utilized an aqueous Ag-Cu electrolyte described previously.¹⁰

ITO substrates were cleaned through sonication in water with 5% Extran solution for 5 minutes followed by sonication in isopropanol for 5 minutes. The substrates were next dried using a stream of air. To modify the ITO surfaces with Pt nanoparticles, the substrates were placed in an ethanolic solution of 10 mM 3-mercaptopropionic acid for approximately 24 hours. Next, the surfaces were rinsed with ethanol followed by water before they were immersed in a solution of Pt nanoparticles that had an average diameter of 3 nm (Sigma-Aldrich) for at least 24 hours. The as-received Pt nanoparticle solution was diluted 1:4 with water before use. After the surfaces were treated with Pt nanoparticles, they were rinsed with water, dried under a stream of air, and annealed in air at 275°C for 20–30 minutes.

Practical full-cell dynamic windows were constructed using one or two working electrodes and one counter electrode. For devices with one working electrode, the working electrode was a 25 cm² Pt-modified ITO on glass substrate, and the counter electrode consisted of Cu foil with a nonconductive glass backing. To ensure uniform electrical contact to the working electrode, Cu tape with conductive adhesive was placed along the electrode perimeter. Butyl rubber was used as a sealant and maintained a ~3 mm spacing between the two electrodes. For devices with two working electrodes, the nonconductive glass backing was replaced with an additional 25 cm² Pt-modified ITO on glass working electrode. The two working electrodes were wired together during device operation. After sealing the devices, an aqueous-based gel electrolyte containing Bi³⁺ and Cu²⁺ ions was injected through the sealant. The electrolyte contained 5 mM BiCl₃, 15 mM CuCl₂, 10 mM HCl, and 1 M LiBr with 3% by weight hydroxylcellulose.

Transmission spectra were measured with an Ocean Optics FLAME-S-VIS-NIR spectrometer coupled with an Ocean Optics DH-mini UV-Vis-NIR light source. Transmission data points were recorded every 100 ms. When plotting spectroelectrochemical data, the transmission and electrochemical data were aligned to have a common timeline using the timestamps provided by the Ocean Optics and Biologic software. Photographs of windows were taken with a Nikon

*Electrochemical Society Member.

^zE-mail: cbarile@unr.edu

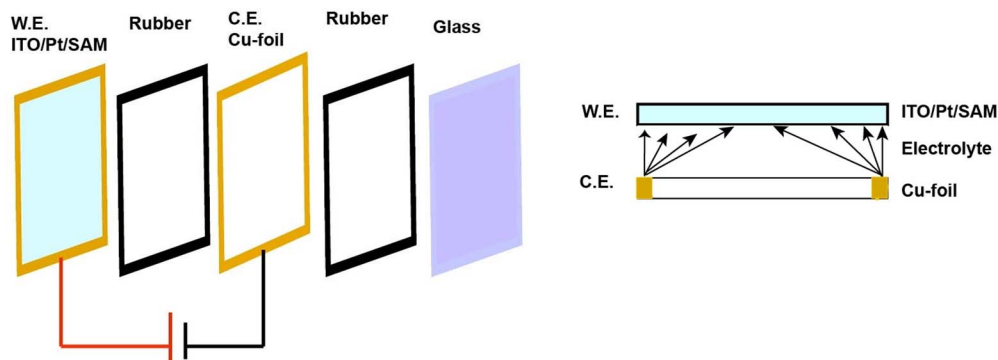


Figure 1. Schematic of the architecture of a dynamic window based on reversible metal electrodeposition that contains one Pt-modified ITO on glass working electrode and a glass back pane. Metal electrodeposition only occurs on the ITO during window tinting.

D5000 Digital Camera. Electrochemical impedance spectroscopy was performed at open circuit potential between 200 kHz and 100 mHz using a voltage amplitude of 10 mV. Scanning electron micrographs (SEM) were obtained using a JEOL JSM-6010LA microscope operated at an accelerating voltage of 20 kV. False coloring was added to the images using Adobe Photoshop.

Patterning on a macroscopic scale was accomplished using Parafilm cut out by hand or an Orafol vinyl sticker cut using a vinyl cutter. The Parafilm or sticker was placed on the ITO on glass before immersing it in the 3-mercaptopropionic acid and Pt nanoparticle solutions. After surface modification, the mask was carefully removed, and a dynamic window was assembled using the patterned Pt-modified ITO as the working electrode. Patterning on a microscopic scale was performed using polystyrene beads (100 μm diameter, Sigma-Aldrich). A cleaned ITO on glass substrate (2 cm by 2 cm) was modified with polystyrene beads by spin-coating a solution containing 80 μL of the as-received polystyrene bead suspension, 80 μL of Polysorbate 20, and 240 μL of water at 1000 rpm for 10 s. This spin-coating process was repeated five times to ensure a dense layer of beads assembled on the surface. After spin-coating, the substrate was annealed in air at 110°C for 1 hour. Metal electrodeposition was elicited using a Ag-Cu electrolyte previously described¹⁰ using chronoamperometry at -0.6 V for 120 s. The surface was rinsed with water and dried with air before SEM imaging.

Results and Discussion

Dynamic windows with one and two working electrodes.—Traditional dynamic windows based on reversible metal electrodeposition utilize the architecture displayed schematically in Figure 1, which has been described previously by Barile et al.^{10,15} During window darkening, a negative voltage is applied to the device with respect to the

Pt-modified ITO working electrode. This voltage causes metal ions in the electrolyte (such as Cu^{2+}) to reduce to elemental metal on the Pt-modified ITO surface. Simultaneously, oxidation occurs at the Cu counter electrode window frame and generates Cu^{2+} . The net reaction during window tinting is therefore the electrochemical movement of metal from the window frame to the Pt-modified ITO electrode. To turn the window clear, a positive voltage is applied to the device with respect to the working electrode, and the opposite reaction occurs and metal is replated on the counter electrode frame.

We sought to improve upon this architecture for metal-based dynamic windows by incorporating a second Pt-modified ITO on glass working electrode (Figure 2). This second working electrode is oriented parallel to the first. With this design, metal electrodeposition can occur simultaneously on both working electrodes, thus improving the contrast ratio and switching speed of the device.

Figure 3 displays a comparison of the transmission changes measured of dynamic windows containing one and two working electrodes that possess a Bi-Cu electrolyte. For the device with a single working electrode, the initial transmission at 600 nm of $\sim 82\%$ decreases to $\sim 30\%$ after 30 s of Bi and Cu electrodeposition at -0.6 V. By comparison, the window with two working electrodes has a similar initial transmission, but decreases to $\sim 15\%$ using the same switching parameters. The increased contrast ratio of the device with double deposition is due to both panes of the window tinting. The contrast ratios of both devices can be improved by increasing the metal electrodeposition time (Figure S1).

To further understand the switching speed of the window containing two working electrodes, we compared the chronoamperometry of the devices during switching (Figure 4). The initial current density and the amount of charge passed through the window with two working electrodes during metal electrodeposition is roughly double the device with one working electrode, as expected. By integrating the total

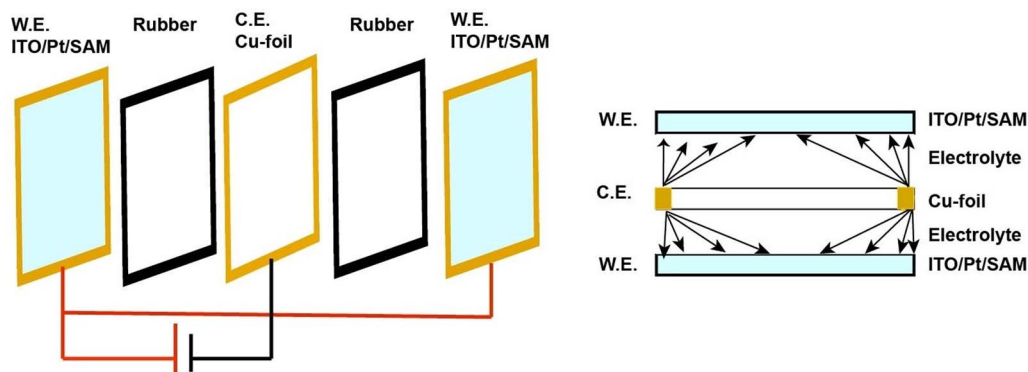


Figure 2. Schematic of the architecture of a dynamic window based on reversible metal electrodeposition that contains two Pt-modified ITO on glass working electrodes. Metal electrodeposition occurs on both ITO electrodes during window tinting.

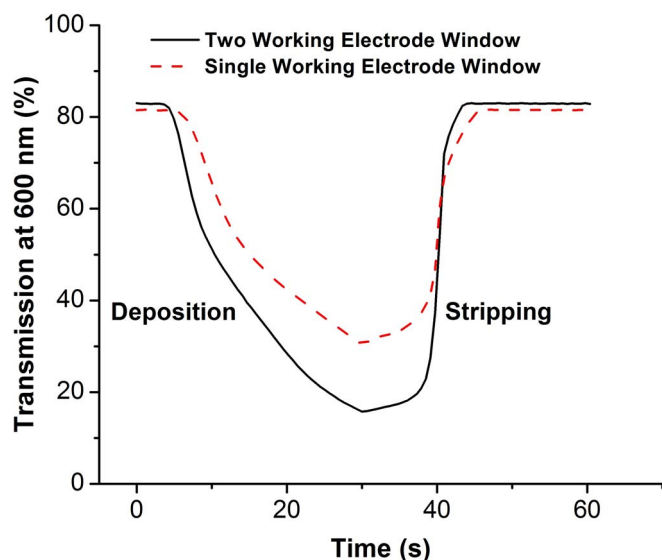


Figure 3. Transmission at 600 nm of 25 cm² metal-based dynamic windows with two (black solid line) and one (red dashed line) working electrodes during switching at -0.6 V for 30 s and $+0.8$ V for 30 s.

charge across the chronoamperometry data, the approximate thickness of the metal electrodeposited on the working electrode can be determined. For the single working electrode case, we calculate that ~ 37 nm of Bi and Cu is electrodeposited after 30 s of device tinting based on a 75% Bi and 25% Cu atomic composition previously determined using X-ray photoelectron spectroscopy for this system.¹⁴ Based on the optical constants of Bi and Cu, a 37 nm thick film of these metals should be almost entirely opaque if the metals are perfectly smooth.¹⁶ In contrast, the transmission of the dynamic window still possesses $\sim 30\%$ transmission after 30 s of electrodeposition (Figure 3, red dashed line) with a metal film that is nominally 37 nm thick. Previous microscopy data, however, demonstrate that the electrodeposited metals on ITO are not smooth on the nanoscale and hence are more transparent than theoretically expected for a smooth metal film.^{10,14}

Modeling the switching speed of a two working electrode window.—Assuming metal electrodeposition occurs at equal rates on

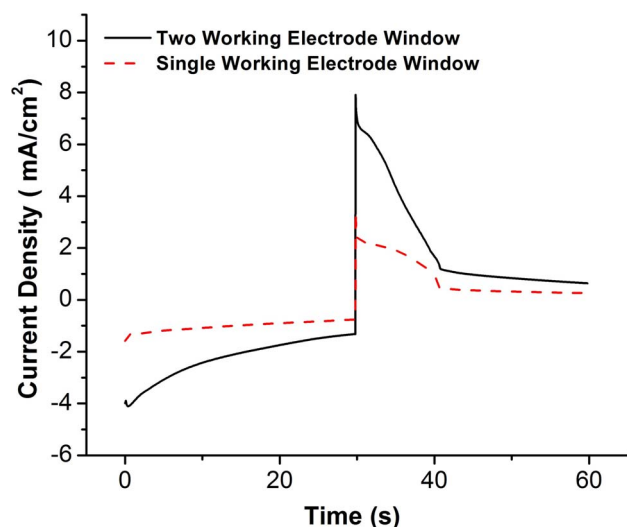


Figure 4. Chronoamperometry of 25 cm² metal-based dynamic windows with two (black solid line) and one (red dashed line) working electrodes during switching at -0.6 V for 30 s and $+0.8$ V for 30 s.

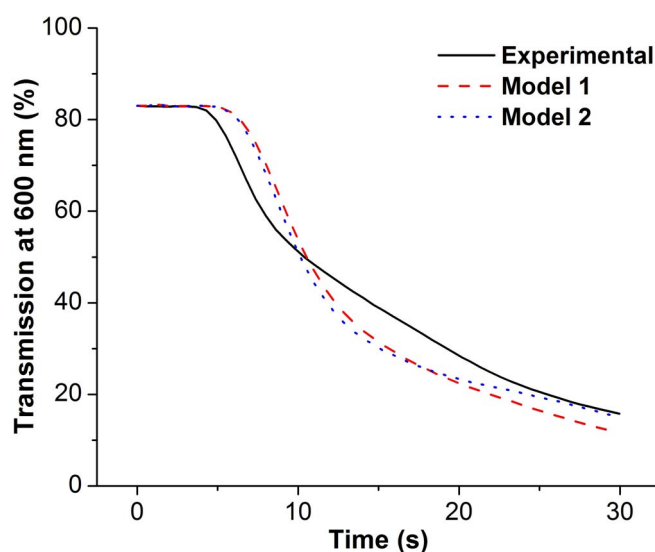


Figure 5. Transmission at 600 nm of a 25 cm² metal-based dynamic window with two working electrodes during switching at -0.6 V for 30 s (black solid line). The red dashed line and blue dotted line represent the predicted transmission curves with Models 1 and 2 depicted in Equations 1 and 2, respectively.

both working electrodes, the switching speed of the window with two working electrodes can be modeled based upon the switching speed of the single working electrode device using Equation 1 below

$$T(t)_{double} = \left(\frac{T(t)_{single}}{T(0)_{single}} \right)^2 T(0)_{double} \quad [1]$$

where $T(t)_{double}$ and $T(t)_{single}$ are the transmissions of windows with two and one working electrodes as a function of time, respectively, and $T(0)_{double}$ and $T(0)_{single}$ are the initial transmissions of the devices. This simple model generates a transmission curve for the double working electrode device that fairly accurately matches the experimental finding (Figure 5, red dashed line compared to black line). To increase the predictiveness of the model, we incorporated the chronoamperometry data into an equation describing the transmission of the window with two working electrodes. The modified Equation 2 is shown below

$$T(t)_{double} = \left(\frac{T(t)_{single}}{T(0)_{single}} \right)^{\frac{i(t)_{double}}{i(t)_{single}}} T(0)_{double} \quad [2]$$

where the newly added variables $i(t)_{double}$ and $i(t)_{single}$ are the current densities as a function of time for the windows with two and one working electrodes, respectively. This second model takes into account slight changes in the relative switching rates between the two devices over time. Experimentally, $i(t)_{double}$ is not exactly twice that of $i(t)_{single}$ and varies from 1.7 to 3 during metal electrodeposition. The predictiveness of this second model is superior to the first (Figure 5, blue dashed line). However, both models do not perfectly match the experimental transmission curve, which was obtained by measuring the transmission of the center of the 25 cm² device. In contrast, the chronoamperometry data are measures of current across the entire device. Since there are slight deviations in the transmission across the entire window area during switching (Figure S2), this discrepancy leads to small inaccuracies in the modeling.

Effect of voltage on metal electrodeposition.—Having understood the behavior of the dynamic windows containing two and one working electrodes, we next sought to increase the switching speed of the devices by increasing the switching voltage. Figure 6 displays a comparison of the transmission curves of devices with two and one working electrodes using -1.2 V for metal electrodeposition instead of -0.6 V. The data for the single deposition device show that the transmission reaches $\sim 30\%$ after 30 s of metal electrodeposition, which is almost

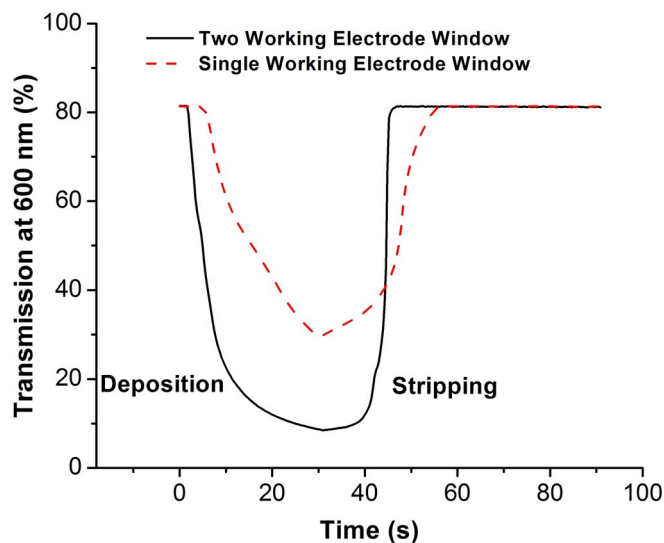


Figure 6. Transmission at 600 nm of 25 cm² metal-based dynamic windows with two (black solid line) and one (red dashed line) working electrodes during switching at -1.2 V for 30 s and $+0.8$ V for 60 s.

identical to the value obtained when -0.6 V is applied (compare Figure 6, dashed red line to Figure 3, dashed red line). At -0.6 V, metal electrodeposition on the Pt-modified ITO working electrode is limited by the diffusion of metal ions to the surface, and further increasing the voltage to -1.2 V does not accelerate metal electrodeposition. Instead, the extra voltage goes toward the H₂ evolution reaction, which results in the formation of bubbles inside the device (Figure S3A-B). In contrast, the switching speed of a device with two working electrodes is increased significantly when the magnitude of the voltage is increased to -1.2 V (Figure 6, blue line). With two working electrodes, the doubled electrode surface area causes the device current to not be diffusion-limited at -0.6 V, and thus increasing the voltage to -1.2 V results in a faster switching time. In this case, the additional voltage goes toward additional metal electrodeposition and not toward the formation of H₂ (Figure S3C-D).

We systematically investigated the effect of electrodeposition voltage on device switching time (Figures S4-S6). An increase in the magnitude of the switching voltage improves the switching time of the device until -1.2 V. Further increasing the switching voltage to -1.5 V causes H₂ formation in both devices with one and two working electrodes and also degrades the ITO electrodes, thus hampering device switch time (Figure S6) and durability.

Having established that -1.2 V is the optimal voltage for switching the window with two working electrodes, we next evaluated the performance of the device using this voltage. Using -1.2 V, the dynamic window with two working electrodes possesses a contrast ratio of $\sim 74\%$ and reaches $\sim 8\%$ transmission at 600 nm in 30 s, making it one of the fastest reported dynamic windows based on metal electrodeposition on the 25 cm² scale.¹⁴ In addition, the transmission profile across visible wavelengths of light is relatively flat, which results in an aesthetically-pleasing black color of the windows in their tinted states (Figure 7). Furthermore, the windows effectively modulate near-infrared light from 700–1300 nm, a property that is useful in controlling heat flow in and out of buildings and automobiles (Figure S7). We note that the electrolyte in the windows absorbs a significant fraction of the light above 1300 nm (Figure S8), thus decreasing the contrast ratio of the devices at these higher wavelengths. We also measured the reflection spectra of the dynamic windows in their clear and opaque states (Figure S9). The windows become more reflective in their opaque state due to increased reflection of light off the electrodeposited metals. However, in both the clear and opaque states, the windows only reflect about 5–25% of light from 300–1500 nm. Although smooth metal films are highly reflective mirrors, the metal electrode-

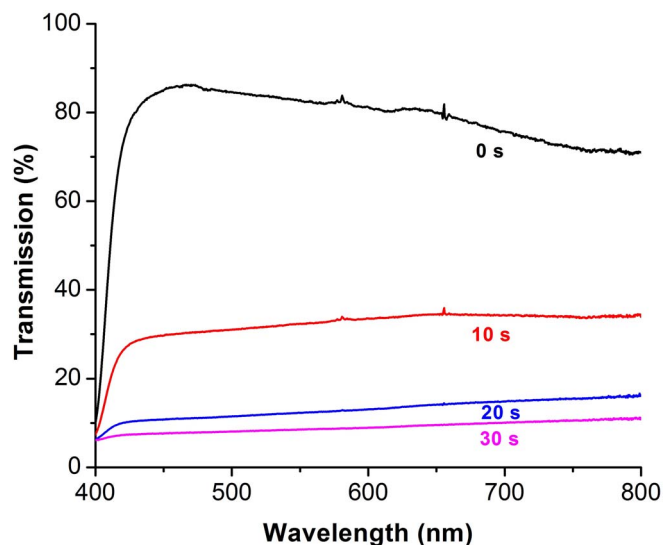


Figure 7. Transmission of a 25 cm² metal-based dynamic window with two working electrodes as a function of wavelength after 0 s (black), 10 s (red), 20 s (blue), and 30 s (pink) of window darkening at -1.2 V.

posited in our devices possesses a rough morphology on the nanoscale that causes the windows to appear black in their opaque state due to increased light absorption.¹⁰ The photographs in Figure 8 demonstrate that a window with two working electrodes switches rapidly and uniformly between clear and black states.

Lastly, we evaluated the cycle life of devices based on reversible metal electrodeposition that contain two working electrodes. Windows with this architecture switch more than 1,000 times without significant degradation in contrast ratio (Figure 9). We chose to switch the windows at -1 V, a less negative voltage than -1.2 V, because we found that a small quantity of H₂ bubbles formed in the devices after several hundred cycles when -1.2 V was utilized. We note that the contrast ratio of the window increases from $\sim 40\%$ to $\sim 60\%$ over the first 100 switching cycles. This increase in contrast ratio could be due to the establishment of stable metal nuclei during initial cycling that facilitate rapid metal electrodeposition during subsequent cycling. Similar small fluctuations in the contrast ratio of metal-based dynamic windows during cycling have been reported previously.¹⁷

In an effort to further understand the different voltage behavior of devices with one and two working electrodes, we performed electrochemical impedance spectroscopy (Figure 10). The impedance spectrum of a device with one working electrode dramatically differs from the spectrum obtained for a device with two working electrodes (Figure 10, black and red). We hypothesize that when the working electrode area is doubled with two working electrodes, the switching kinetics become limited by reactions on the counter electrode. To test this hypothesis, we calculated the resistance of the counter electrode for the different device architectures using the first equivalent circuit previously discussed by Nara et al. for full cell devices.¹⁸ The calculated resistance of the counter electrode increases from 29 Ω to 53 Ω when

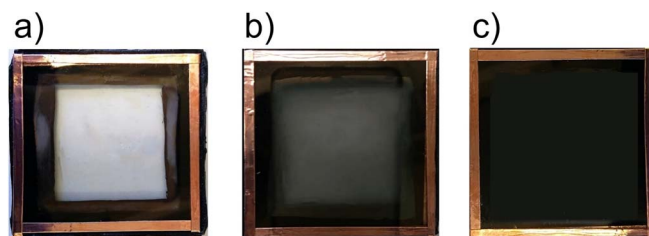


Figure 8. Photographs of a 25 cm² metal-based dynamic window during switching at -1.2 V for 0 s (a), 15 s (b), and 30 s (c).

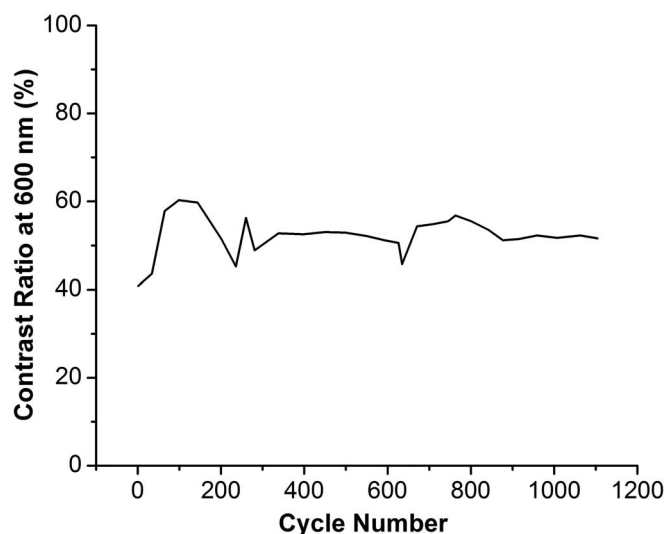


Figure 9. Contrast ratio at 600 nm during more than 1,000 cycles of a dynamic window based on reversible metal electrodeposition with two working electrodes.

increasing the number of working electrodes from one to two. With two working electrodes, more IR drop occurs on the counter electrode due to its higher resistance, and thus the voltage that goes to the electrolyte to induce metal electrodeposition is diminished. In contrast, with one working electrode, the IR drop through the counter electrode is less, and so more voltage is applied to the electrolyte. This difference in IR drop explains why applying -1.2 V to the single deposition device causes H_2 formation, but the device with two working electrodes does not produce H_2 (Figure S3).

Window patterning.—As discussed in the Introduction, a SAM of Pt nanoparticles is used on the working electrode to provide an even distribution of nucleation sites and elicit uniform metal electrodeposition across the 25 cm^2 device area. The Pt nanoparticles act as nucleation sites because metal electrodeposition occurs more readily on another metal such as Pt than on heterogeneous metal oxide surfaces like ITO. For example, cyclic voltammograms conducted in a Ag-Cu electrolyte indicate that metal electrodeposition occurs more readily

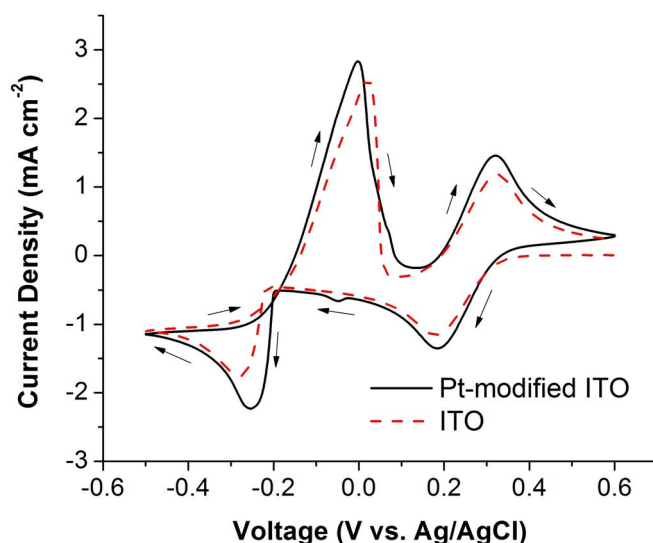


Figure 11. Cyclic voltammograms in a Ag-Cu electrolyte using a Pt-modified ITO on glass (black solid line) and unmodified ITO on glass (red dashed line) working electrode at 20 mV/s .

on Pt-modified ITO than unmodified ITO (Figure 11). On both electrodes, the peaks centered at about $+0.25\text{ V}$ are due to the Cu(II)/Cu(I) redox couple. At about -0.25 V , there is a sharp increase in cathodic current due to metal electrodeposition. However, the onset potential for metal electrodeposition on the Pt-modified ITO electrodes occurs about 30 mV more positive than on the unmodified ITO electrode, indicating that it is more favorable for metal electrodeposition to occur on the Pt nanoparticles. The peaks at about 0 V on both electrodes are due to stripping of the electrodeposited metals.

The difference in the onset potentials for metal electrodeposition on the Pt-modified and unmodified ITO electrodes suggests that it is possible to selectively electrodeposit metal on the SAM of Pt nanoparticles. To test this hypothesis, we constructed dynamic windows with ITO working electrodes that were patterned with Pt nanoparticles through masked self-assembly. By covering the ITO substrate with a mask (e.g. a hand-cut N-shaped piece of Parafilm wax or a vinyl-cut tree-shaped sticker) during Pt SAM formation, the Pt SAM is formed only on portions of the ITO electrode not covered by the mask. The photographs

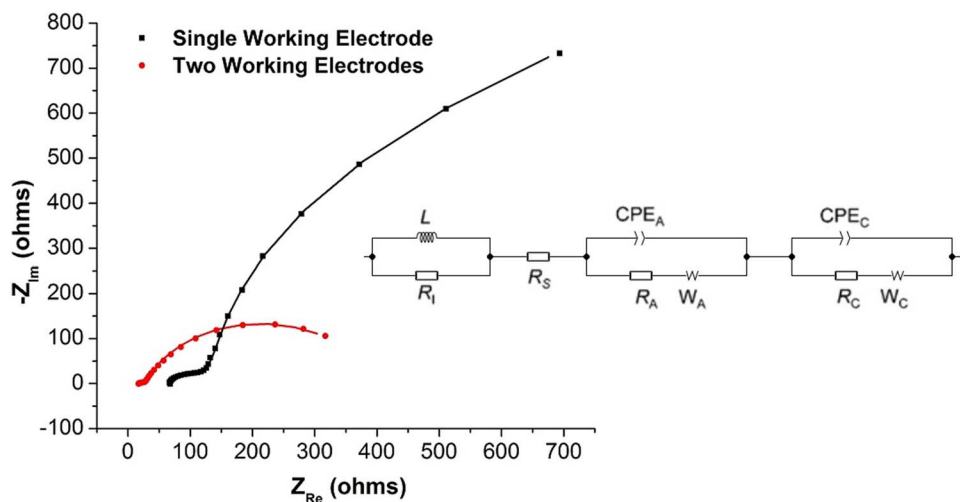


Figure 10. Electrochemical impedance spectroscopy of 25 cm^2 metal-based dynamic windows with one (black) and two (red) working electrodes. The solid lines represent best fits from the shown equivalent circuit where L and R_1 are an inductor and a resistor associated with contact wiring, R_S is the resistance of solution, CPE_A , CPE_C , R_A , R_C , W_A , and W_C are constant phase elements, resistors, and Warburg elements for the anode (A) and cathode (C), respectively. The resistances of the counter electrode anode (R_A) were calculated to be $29\ \Omega$ and $53\ \Omega$ for these two devices, respectively.

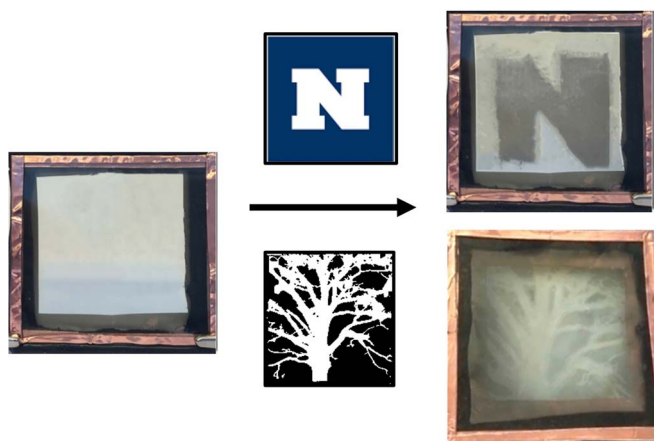


Figure 12. Photographs of a 25 cm² dynamic window in its clear state (left) and after 60 s of metal electrodeposition at -0.6 V using ITO on glass working electrodes with two different patterns of SAMs of Pt nanoparticles (right).

in Figure 12 demonstrate that the darkening of 25 cm² dynamic windows containing these patterned working electrodes occurs only in areas where the Pt SAM is present, indicating that reversible metal electrodeposition devices can be constructed with electrodeposition occurring in any desired pattern on a macroscopic scale.

Having demonstrated the ability to macroscopically pattern reversible metal electrodeposition, we next evaluated if selective electrodeposition could also be elicited on the microscale. Figure 13 shows a schematic of how we fabricated a micropatterned Pt SAM. First, spherical polystyrene (PS) beads 1 μ m in diameter were spin-coated on ITO-coated glass to give close-packed clusters of beads as indicated by optical microscopy (Figure 14A). Next the PS-modified surface was immersed in a solution of 3-mercaptopropionic acid to form

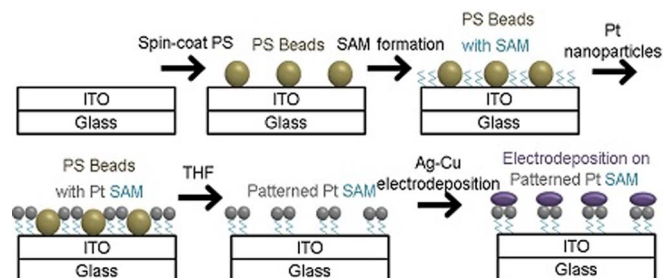


Figure 13. Schematic showing the fabrication of micro-patterned metal electrodeposition with a SAM of Pt nanoparticles templated by polystyrene beads.

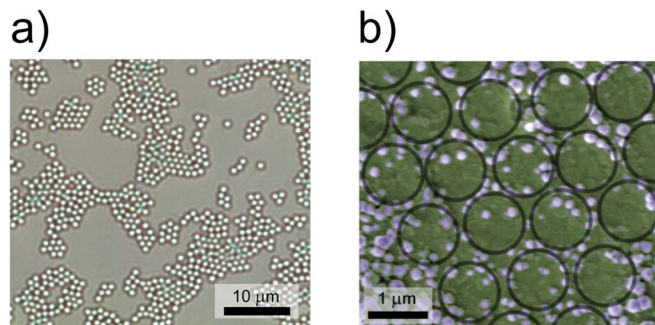


Figure 14. Optical microscopy of 1 μ m polystyrene spheres spin-coated on ITO on glass (a). False-color SEM image of Ag-Cu electrodeposits (b, purple particles) on ITO with a Pt SAM patterned with 1 μ m polystyrene spheres. The Pt SAM does not deposit where the polystyrene spheres once were (indicated by black circles), leaving bare ITO (b, green background). For the most part, the Ag-Cu electrodeposits grow selectively on the Pt SAM.

a SAM followed by a solution of Pt nanoparticles, which covalently bind to the thiol groups of the SAM. The PS beads were subsequently removed by immersing the surface in THF to yield the patterned Pt SAM electrode. The false color SEM image in Figure 14B shows that electrodeposition of Cu and Ag (colored purple) occurs in the void spaces left by the mask of the close-packed PS spheres (black circles). This result indicates that selective metal electrodeposition using patterned Pt SAMs can also be performed on the microscale.

The ability to pattern reversible metal electrodeposition for dynamic windows on the microscale could be used to tune the optical properties of metal-based dynamic windows. For example, reversible diffraction gratings, which have applications in various optical devices,¹⁹ could be constructed by patterning the Pt SAM on the microscale in the shape of diffraction gratings. Further improvements of the concept shown here could enable nanoscale electrodeposition patterning, which would allow for device optics to be tuned through plasmonic effects if a plasmonically active metal such as Ag is electrodeposited.

Conclusions

In conclusion, we have demonstrated that there is significant flexibility in the architecture of dynamic windows based on reversible metal electrodeposition. The use of a metal frame counter electrode allows windows with two working electrodes to be constructed. Since metal electrodeposition occurs on both window panes, these devices possess superior contrast ratios to their single deposition counterparts. We also show that metal electrodeposition selectively occurs on the Pt nanoparticles used to modify ITO electrodes. This selectivity enables the patterning of reversible metal electrodeposition on both the macroscopic and microscopic scale.

Acknowledgments

This research was funded by Research and Innovation at the University of Nevada, Reno.

ORCID

Christopher J. Barile <https://orcid.org/0000-0002-4893-9506>

References

1. L. Perez-Lombard, J. Ortiz, and C. Pout, *Energy Buildings*, **40**, 394 (2008).
2. S. E. Lee and M. Yazdani, *Lawrence Berkeley National Laboratory*, LBNL-54966 (2004).
3. Energy Benefits of View Dynamic Glass in Workplaces. *View Glass* (2017), <https://viewglass.com/assets/pdfs/workplace-white-paper.pdf> accessed 10/12/18.
4. V. K. Thakur, G. Ding, J. Ma, S. P. Lee, and X. Lu, *Adv. Mater.*, **24**, 4071 (2012).
5. C. M. Amb, A. L. Dyer, and J. R. Reynolds, *Chem. Mater.*, **23**, 397 (2011).
6. L. Bouteiller and P. L. Barny, *Liq. Cryst.*, **21**, 157 (1996).
7. J. Murray, D. Ma, and J. N. Munday, *ACS Photonics*, **4**, 1 (2017).
8. M. Kamalifarvestani, S. Rahman, S. Mekhilef, and F. S. Javadi, *Renew. Sust. Energy Rev.*, **26**, 353 (2013).
9. H. Kim, Y. Kim, K. S. Kim, H. Y. Jeong, A. R. Jang, S. H. Han, D. H. Yoon, K. S. Suh, H. S. Shin, T. Kim, and W. S. Yang, *ACS Nano*, **7**, 5769 (2013).
10. C. J. Barile, D. J. Slotcavage, J. Hou, M. T. Strand, T. S. Hernandez, and M. D. McGehee, *Joule*, **1**, 133 (2017).
11. G. K. A. Alcaraz, J. S. Juarez-Rolon, N. A. Burpee, and C. J. Barile, *J. Mat. Chem. C*, **6**, 2132 (2018).
12. J. P. Ziegler and B. M. Howard, *Sol. Energy Mater. Sol. Cells*, **39**, 317 (1995).
13. J. P. Ziegler, *Sol. Energy Mater. Sol. Cells*, **56**, 477 (1999).
14. T. S. Hernandez, C. J. Barile, M. T. Strand, T. E. Dayrit, D. J. Slotcavage, and M. D. McGehee, *ACS Energy Lett.*, **3**, 104 (2018).
15. C. J. Barile, *J. Appl. Electrochem.*, **4**, 443 (2018).
16. O. S. Heavens, *Optical Properties of Thin Solid Films*, Dover Publications, New York, (1965).
17. S. M. Islam, T. S. Hernandez, M. D. McGehee, and C. J. Barile, *Nat. Energy*, **4**, 223 (2019).
18. T. Osaka, T. D. Momma, D. Mukoyama, and H. Nara, *J. Power Sources*, **205**, 483 (2012).
19. C. A. Tippets, Q. Li, Y. Fu, E. U. Donev, J. Zhou, S. A. Turner, A. M. Jackson, V. S. Ashby, S. S. Sheiko, and R. Lopez, *ACS Appl. Mater. Interfaces*, **7**, 14288 (2015).